The study of polycrystalline nickel metal oxidation by water vapour

B.P. Payne [a,*], M.C. Biesinger [b], N.S. McIntyre [a]

[a] *Department of Chemistry, The University of Western Ontario, London, ON N6A 5B7, Canada*
[b] *Surface Science Western, The University of Western Ontario, London, ON N6A 5B7, Canada*

ARTICLE INFO

ABSTRACT

The oxidation of polycrystalline nickel (Ni) metal surfaces with water (H_2O) vapour was studied at 25 °C and 300 °C using dose rates considerably higher than in previous studies. The reaction rate was followed to a point where the oxide thickness was several nanometers. This was done using X-ray photoelectron spectroscopy (XPS) and modeling of the spectral profiles using QUASES[TM]. The surface reaction rate is much slower than that with oxygen gas (O_2) and it terminates within a few nanometers. The films formed were found to be composed of a defective nickel oxide (NiO) containing both divalent nickel (Ni^{2+}) and trivalent nickel (Ni^{3+}) as had been observed previously for reaction of Ni with O_2. The reason for the much slower reaction rate in the case of H_2O vapour appears to be linked to a slower place exchange with a surface hydroxyl (OH (ads)) intermediate. This adsorbate species appears only to be stabilised on metallic Ni and termination of oxide growth is believed to occur once all the available surface metal sites have been covered with oxide.

© 2009 Elsevier B.V. All rights reserved.

1. Introduction

The reaction of nickel (Ni) metal surfaces with water (H_2O) vapour has been found to be much slower than with gaseous oxygen (O_2) [1]. This difference is important in view of the corrosion-resistant nature of Ni and its alloys. Previous studies of the Ni–H_2O reaction have used single crystals and low doses and dose rates of water [1–6].

The initial reaction of single crystal Ni (1 0 0) surfaces and H_2O vapour was studied using XPS by Benndorf et al., particularly at low temperatures [2,3]. At temperatures below −120 °C adsorbed water molecules (H_2O (ads)) were the sole source of an O 1s signal with a binding energy (BE) that increased with increasing dose (533.1–534.4 eV) [3]. This shift was attributed to a decrease in the oxygen (O)–surface interaction due to the formation of multiple layers of hydrogen (H)-bonded clusters of H_2O molecules. At higher temperatures, formation of an O 1s oxidic peak was observed, along with peaks in the BE range of 532.6–532.8 eV. The possibility of adsorbed hydroxide (OH (ads)) was eliminated using isotope exchange measurements. It was concluded that the reaction occurred by H_2O (ads) dissociating into adsorbed atomic oxygen (O (ads)) and hydrogen gas (H_2).

The reaction of H_2O vapour with clean as well as oxygen (O) pre-covered single crystal Ni (2 1 0) metal surfaces was also studied by Carley et al. using XPS at low temperatures [6]. After adsorption of H_2O at temperatures below −100 °C, heating of the surface resulted in an O 1s peak at 531.5 eV, which is attributed to the formation of OH (ads) species. The group of Norton et al. also exposed clean and pre-covered single crystal Ni (1 0 0) and (1 1 1) metal surfaces to H_2O vapour, O_2 gas and air containing H_2O at temperatures near 20 °C [1]. The reactivity of clean single crystal metal surfaces was determined to be almost 10^3 times less reactive towards H_2O vapour than O_2 gas. Reactions of clean or pre-oxidised Ni with H_2O vapour at ambient conditions produced a new peak at 531.3 eV [1]. The presence of any nickel hydroxide (Ni(OH)$_2$) species was eliminated using nuclear reaction analysis. Rather, the authors proposed a dinickel trioxide (Ni_2O_3)-like species with some involvement by H.

A study from this laboratory of the equivalent H_2O vapour–iron (Fe) reaction [7,8] has identified OH groups as one product of the reaction and has suggested that their subsequent decomposition produces H atoms that could assist in blocking migration of cations to the surface [7–9].

From the studies described above it can be seen that the surface products of this very important Ni reaction are still ambiguous. Much of this is due to differing interpretations of XPS O 1s spectra of the products. Such spectra are potentially the single most useful means for identifying different products, but unfortunately there have been large uncertainties both with the species represented as well as with their line positions.

* Corresponding author at: Department of Chemistry, The University of Western Ontario, Rm 227D Physics and Astronomy Building, London, ON N6A 5B7, Canada. Tel.: +1 519 661 2111x86703.
  E-mail address: bpayne2@uwo.ca (B.P. Payne).

This paper reports another study of the Ni–H_2O vapour reaction. In addition to a study of the kinetics of oxide growth over an exposure regime much wider than the previous studies, the present work undertakes a detailed analysis of possible interpretations of the O 1s spectra associated with each reaction.

Most of the surface characterisation done in this work was carried out using XPS and algorithms developed by Tougaard [10]. These algorithms have been incorporated into a software package called QUASES[TM], which is separated into two analytical routines 'Analyze' and 'Generate' [11]. The 'Analyze' program can be used to determine the thicknesses of surface overlayers, such as oxide films, by modeling the depth from which the detected photoelectrons originated. The 'Generate' program maps the atomic distribution throughout the surface using a combination of reference spectra whose extrinsic backgrounds have been modified as a result of the depth from which they are located [11,12]. Similar oxidation studies using Ni and O_2, as well as Fe and O_2, and Fe and H_2O have been completed using this same program [7,8,12–16].

In this paper the oxidation of Ni metal surfaces was studied following doses of up to 3.0×10^{10} Langmuir (L) of H_2O vapour at pressures around 130 Pa and temperatures of 25 °C and 300 °C. The pressure of the vapour reactant used here is many orders of magnitude higher than those used in most surface reaction studies. Pressure differences have been shown to change the reaction mechanism in other surface oxidation studies [13,17]. In fact, the pressures used here are within a few orders of magnitude to those used in liquids.

2. Experimental

Polycrystalline Ni metal samples were cut into 3.4 mm thick discs from a polycrystalline rod (Alfa Aesar, 99.995% pure) and one face was polished to a mirror finish using 0.05 μm γ-Al_2O_3 paste. The size of the grains found on each surface typically ranged from 70 to 175 μm in diameter. From a qualitative analysis of texture using SEM to compare channeling contrast, the distribution of contrasting grain shades appeared to be relatively even. From a previous study it was suggested that grain boundaries play a dominant role in the outward transport of Ni cations and that the character of the boundaries is likely to play a more important role here than the orientation(s) of the grain faces themselves [14]. After polishing, the samples were sonicated in methanol and then placed into an isolated chamber in a Kratos AXIS Ultra XPS having base pressures ranging between 4×10^{-6} and 7×10^{-7} Pa for surface cleaning. All Ni metal samples were argon ion (Ar^+) sputtered for 15 min using a 4 kV beam with an emission current of 15 mA. Following sputter cleaning, the samples were annealed at 600 °C for 30 min. The roughness of the surfaces following ion bombardment and annealing was not measured however, examination of these surfaces showed brightened regions where the sputtering had occurred. During the annealing process the chamber pressure increased to around 3×10^{-5} Pa. To verify that an atomically clean surface had been obtained (no detectable impurities) the samples were transferred under vacuum to an analytical chamber, having pressures close to 7×10^{-7} Pa, where XPS survey scans were collected. The survey scans showed that surface contamination from either O or carbon (C) was no more than 0.3 atom %.

All oxidation experiments were carried out in a reaction chamber attached to the XPS instrument having a base pressure of 7×10^{-6} Pa. Prior to any vapour exposures, a Residual Gas Analyser (RGA), a quadrapole mass spectrometer, was used to monitor the amount of contaminate gases present. The Ni metal surfaces were then exposed to doses of H_2O vapour that had been heated to remove as much O_2 and carbon monoxide (CO) as possible. Any remaining contaminant gas was removed through multiple freeze–pump–thaw cycles. After several cycles, the amount of O_2 present in the H_2O container was undetectable by RGA analysis. The H_2O vapour exposures were carried out at 25 °C and 300 °C for doses of 1.2×10^9, 3.0×10^9, 3.6×10^9, 8.4×10^9 and 3.0×10^{10} L. The pressures in the reaction chamber were measured using a combination Pirani and Penning gauge.

All Ni metal surfaces were analysed using both monochromatic Al Kα and achromatic Zr Lα X-ray sources. The XPS survey scans were collected using the following parameters: hybrid focussing lens, pass energy = 160 eV, an energy step size = 0.7 eV, charge neutraliser = 1.6 A and 2.4 eV, and the slot beam size (700 μm × 300 μm). The Al Kα spectra were taken over a binding energy (BE) range = 1100–0 eV, a scan time = 180 s, and the number of sweeps = 10. The Zr Lα excited scans were acquired over a BE range = 1800–0 eV, a scan time = 360 s, and the number of sweeps = 20. High-resolution XPS analysis of the Ni 2p, O 1s, and C 1s envelopes used Al Kα excitation only at pass energy = 20 eV over energy windows ranging between 20 and 40 eV, depending on the element being analysed. An analysis region of 700 μm × 300 μm would encompass an area involving 8–10 separate crystals based on the grain sizes stated above.

CasaXPS Version 2.3.14 was used for the analysis of all the XPS spectra [18]. The surface atomic % of each element present was determined using XPS survey spectra. The total amount of Ni on each surface was calculated using the area of the Ni $2p_{3/2}$ peak only [18]. To monitor the oxide composition, high-resolution XPS was employed on the Ni 2p, O 1s, and C 1s regions. Relative elemental concentrations were determined using Scofield cross-sections corrected for the kinetic energy of the particular photoelectrons. This was particularly useful for estimating surface coverage of the metal.

It was determined that each Ni surface contained small amounts of adventitious carbon (C (adv)) on the surface; this was used for spectral calibration as the C (adv) peak was set to a BE of 284.8 ± 0.1 eV. Each C 1s spectrum also showed the presence of three additional C species centred at 286.3 ± 0.2 eV, 287.7 ± 0.1 eV and 288.6 ± 0.1 eV (see Fig. 1(a)). These peaks are assigned to alcohol (–COH), carbonyl (–CO) and ester (–COO–) functional groups, respectively [19]. The identification of these adsorbate species becomes important when analysing the O 1s spectra (Fig. 1(b)), as they will also add to the observed photoelectron signal here, and thus complicate the analysis of this spectrum. Four small peaks associated with O-containing adsorbates are visible at higher BE in most O 1s spectra; all their intensities are tied to those in the corresponding C 1s spectrum. Fig. 1(c) shows an expanded view of this region illustrating more clearly the BE positions of the –COH (532.7 ± 0.2 eV), –CO (532.1 ± 0.1 eV) and –COO– (532.1 ± 0.3 eV, 533.6 ± 0.1 eV) adsorbate species [19].

The CasaXPS software was also used for spectral subtractions; in these the contribution from the Ni metal substrate was removed to reveal the underlying structures resulting from oxidation. Each subtraction entailed a normalising of the intensity of a clean Ni metal reference component having a BE of 852.6 eV (Fig. 2(a)) with the intensity of the same peak found on the oxidised scans. A second subtraction was then undertaken to remove the nickel oxide (NiO) contribution this time by normalising the intensity of the main NiO line at 854.0 ± 0.2 eV. Care had to be taken to separate the correction of the charging components (oxides) from those of the metallic substrate. An identical method for spectral analysis was reported in previous publications [14,20]. Fig. 2(b and c) also contains the high-resolution spectra of powdered polycrystalline NiO and Ni(OH)$_2$. Both powders contain divalent nickel (Ni^{2+}) species, however the shapes of the two main lines are distinctly different [21]. Spectra of possible trivalent (Ni^{3+}) structures, such as gamma and beta nickel oxy-hydroxide (γ-NiOOH, β-NiOOH) are presented in Fig. 3(a and b).
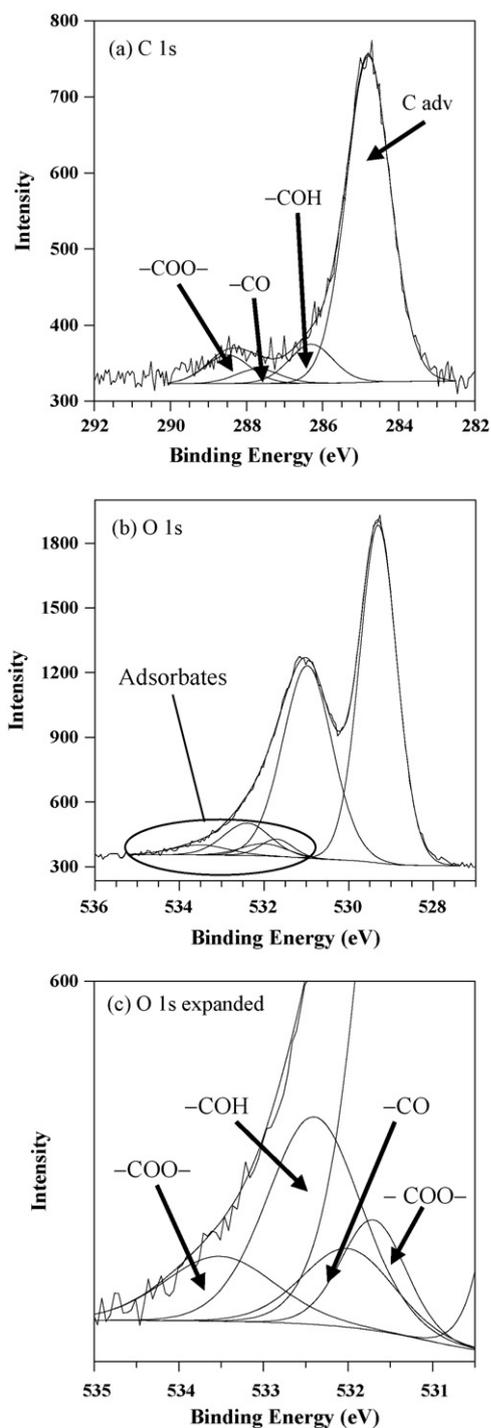
Fig. 1. High-resolution spectrum of the C 1s region of a Ni metal surface exposed to H_2O vapour showing the BE shifts of the C (adv), –COH, –CO and –COO– species (a). The corresponding peak positions in the O 1s region for the –COH, –CO and –COO– species are shown in (b), with an expanded view of this region shown in (c).

Comparison of the Ni spectra in Figs. 2 and 3 shows an overlap between the Ni $2p_{1/2}$ peak of the clean metal scan with the satellite structure in the Ni $2p_{3/2}$ portion of the NiO, $Ni(OH)_2$ and both NiOOH standard spectra. This overlap must be taken into account to accurately analyse surfaces containing Ni metal along with one or more oxidised Ni species. All Ni 2p envelopes collected as a part of this study were subject to analysis using the Ni metal, NiO, $Ni(OH)_2$ and NiOOH peak fitting parameters presented recently by Biesinger et al., where the BE of each peak was allowed to drift by ± 0.1 eV

[20]. The fits developed by Biesinger et al. employ an off-set in the Shirley background to more accurately model the Ni 2p spectra of surfaces containing both metallic and oxidised species.

The corresponding O 1s spectra for the NiO and $Ni(OH)_2$ powders are shown in Fig. 2(d and e). The NiO powder appears to contain two major O species at 529.3 eV and 531.0 eV. The BE of the first peak is assigned to O bonded within a regular oxide crystal (O^{2-}) and the second is assigned to oxygen atoms in positions adjacent to Ni vacancies (O (def)) within the oxide structure. Similar assignments of this peak have been made previously by several other authors [1,20,22–25]. In the case of the $Ni(OH)_2$ powder only one major O species at 531.1 eV is evident and is assigned to a hydroxide bound to Ni (OH^-). Fitting of the γ-NiOOH O 1s spectrum (Fig. 3(c)) showed both O^{2-} and OH^- signals at 529.5 eV and 531.1 eV, respectively. The same two O^{2-} and OH^- components appear in the β-NiOOH spectrum (Fig. 3(d)) with BE shifts of 529.3 eV and 530.8 eV, respectively. All the O 1s envelopes were also fit with the four small peaks associated with the C and O adsorbates mentioned previously. A more detailed analysis of these spectra is given in Appendix A.

Further analysis of the oxidised surfaces was carried out using algorithms that were developed by Tougaard [10]. The basis of the Tougaard approach is that photoelectrons moving through a surface can undergo multiple scattering events prior to escaping to the vacuum phase. These energy loss interactions lead to the formation of the background found on the low kinetic energy (KE) side of the peaks in XPS spectra [10]. The shape of the background is defined by the distribution of atoms within the near surface region. Modeling of these structures can be undertaken using one of the five depth concentration profiles that are included with the QUASES^{TM} software package; 'buried layer', 'island active substrate', 'islands passive substrate', 'exponential profile', or 'several buried layers' [12]. For the purposes of this work both the 'buried layer' and 'island active substrate' profiles were employed during surface analysis. The 'buried layer' profile models the energy lost by the photoelectrons emitted from atoms contained within in a homogenous layer as they pass through an overlying material having a different composition. The 'island active substrate' models the extrinsic losses of photoelectrons emitted from substrate atoms as they pass through overlying islands. These islands do not have to be uniform in size and/or shape [12]. The probability that an electron emitted from an atom located at a certain depth will reach the surface is dependent on both a material-specific inelastic mean free path (IMFP) and the energy loss cross-section. The latter term simply represents both the likelihood the photoelectron would undergo a scattering event as well as the average energy lost per collision [10]. The IMFP values for the different Ni-containing species were calculated using the NIST Electron Inelastic Mean Free Path Database (Version 1.1) [26] software, which uses the TPP-2M equation [27]. Previous IMFP calculations completed by this group were then subsequently shorted by 20% to give the actual photoelectron attenuation length (AL) [14]. It was later determined that the IMFPs estimated as part of Ni–O_2 work were calculated incorrectly. The current IMFPs calculated as part of this work compare well to the ALs presented in reference [14] and are now used for analysis of all oxide films. The same database was used by Biesinger et al. to determine their IMFP values [20].

Sample oxide thicknesses were calculated with the 'Analyze' program using an IMFP of 1.4 nm and the O 1s region of XPS survey spectra excited with Al Kα X-rays. The oxide surface structures were modeled using 'Generate', and the Ni 2s peak collected from Zr Lα excited scans. Each sample was fit using reference spectra acquired from a clean polycrystalline Ni metal surface and a sample of powdered polycrystalline NiO. Photoelectron IMFPs of 1.4 nm and 1.5 nm were calculated for the metal and NiO standards, respectively. All QUASES^{TM} 'Generate' analysis used a Ni-specific energy loss cross-section that was calculated by Tougaard [14].
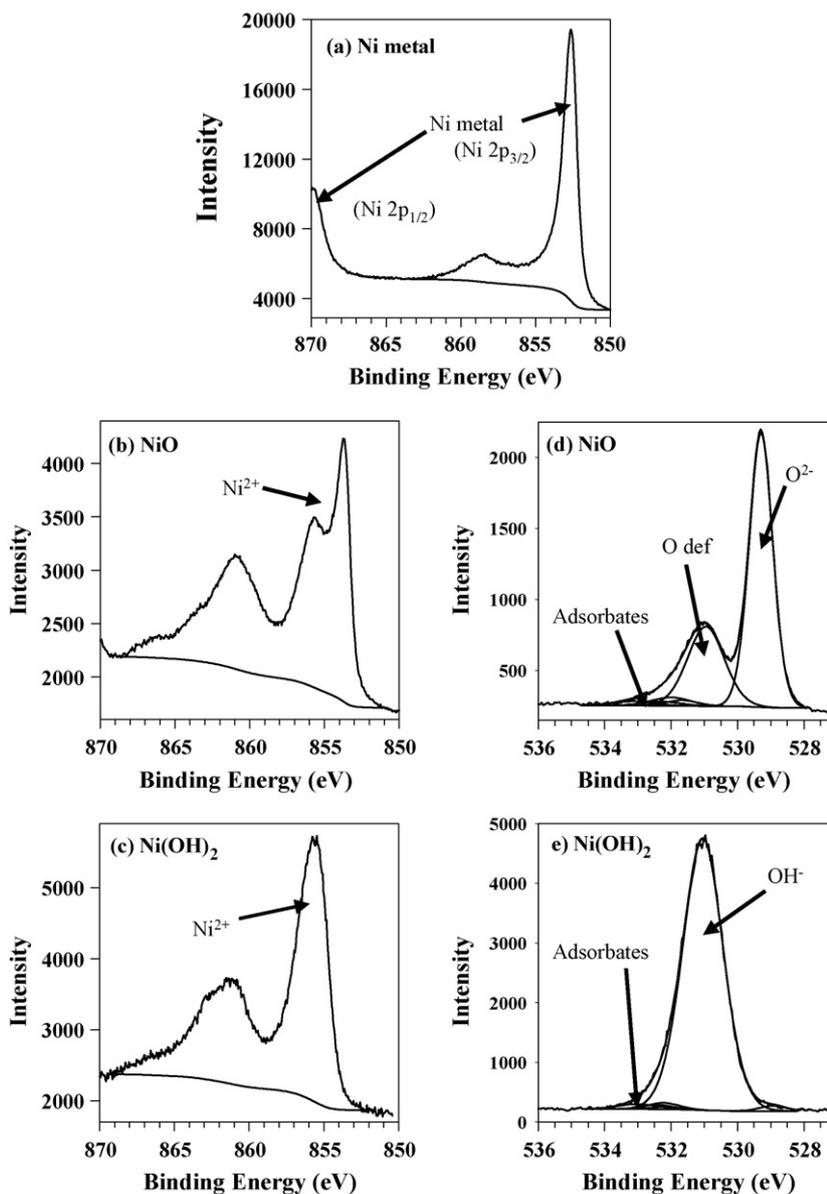
Fig. 2. High-resolution Ni $2p_{3/2}$ spectra of (a) a clean Ni metal surface, (b) a polycrystalline NiO powder and (c) a polycrystalline Ni(OH)$_2$ powder. High-resolution O 1s spectra of (d) NiO and (e) Ni(OH)$_2$. Part of the metal Ni $2p_{1/2}$ line can be observed in (a).

The QUASES^{TM} 'Analyze' results were verified using the Strohmeier method [28]. The Strohmeier overlayer equation is given below:

$$d = \lambda_0 SIN\Theta \ln \left[\frac{N_m \lambda_m I_o}{N_o \lambda_o I_m} + 1 \right] \tag{1}$$

where d represents the thickness of the overlayer, λ_o is the photoelectron IMFP, m and o denote the metal and oxide components respectively derived from fitted high-resolution XPS spectra, N stands for the volume density of metal atoms in either the metal or the oxide phase, I is the peak area for either the metal or the oxide, and Θ is the take off angle of the electrons.

For a study using ToF-SIMS, a sample of polycrystalline Ni metal was cut from the same rod above and polished with 0.05 μm γ-Al$_2$O$_3$ paste. Following polishing, the sample was sonicated in methanol then introduced into an ION-TOF (GmbH) ToF-SIMS IV single-reflection mass spectrometer. The surface was sputtered using a 3 kV Ar$^+$ beam with a 140 nA target current for 8100 s.

After sputtering, the surface was heated into the range of 300–400 °C, and then exposed to H$_2$O vapour containing high-

purity deuterium (D) for 20 min ($\sim$1.2 × 10^9 L) at an average pressure of 130 Pa. During the dose, the pressure dropped to as low as 10 Pa, and spiked to as high as 530 Pa for no more than a few seconds. D$_2$O was used instead of H$_2$O because of the high probability of H contamination from within the vacuum system. A shallow depth profile into the surface was collected using the dual beam mode, monitoring negative secondary ions. The analysis beam was a 25 kV pulsed bismuth ion (Bi$^+$) with a 0.5 pA target current, rastered over a 200 μm × 200 μm area. The sputter beam was a 3 kV cesium ion (Cs$^+$) rastered over 500 μm × 500 μm with a target current of 10 nA. The Bi$^+$ analysis region was centred within the Cs$^+$ sputter crater to avoid edge effects. The ToF-SIMS results were analysed using the IONSPEC program [29].

3. Results and discussion

Fig. 4 contains Ni $2p_{3/2}$ high-resolution spectra collected from metal surfaces exposed to H$_2$O vapour at 300 °C for doses of 1.2 × 10^9, 3.6 × 10^9, 8.4 × 10^9 and 3.0 × 10^{10} L. A small contribution from the metal Ni $2p_{1/2}$ peak is visible on all spectra at high BE.

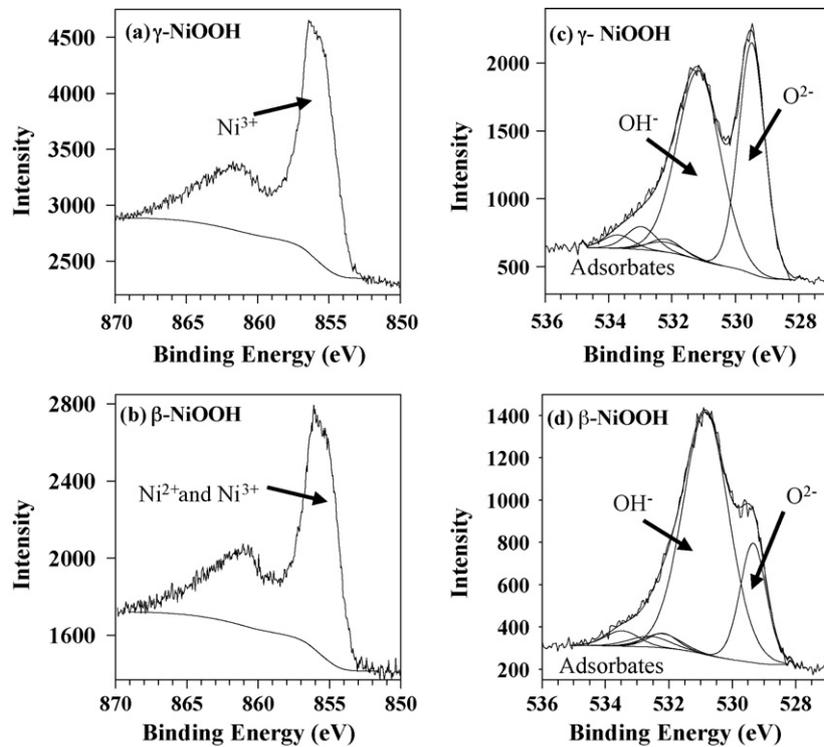**Fig. 3.** High-resolution Ni 2p$_{3/2}$ spectra of (a) γ-NiOOH and (b) β-NiOOH powders. High-resolution O 1s spectra of (c) γ-NiOOH and (d) β-NiOOH.

With continuing exposure time, an increase in the Ni 2p line shape and background was observed as a result of surface oxidation. The intensity of the Ni metal peak found in the Ni 2p spectra in Fig. 4 makes it difficult to observe, in its entirety, the line shape of the oxidised species. The metal contribution was therefore removed and the subtracted spectra for the 3.6×10^9, 8.4×10^9 and 3.0×10^{10} L

exposures are shown in Fig. 5(a–c). Subtraction of the metal component from the surface exposed to 1.2×10^9 L produced a very noisy spectrum (not shown), indicating that very little oxidation has occurred. From the subtracted spectra, the characteristic shape and BE positions of NiO suggests it to be the major non-metal phase present for these doses. However, the intensities under the
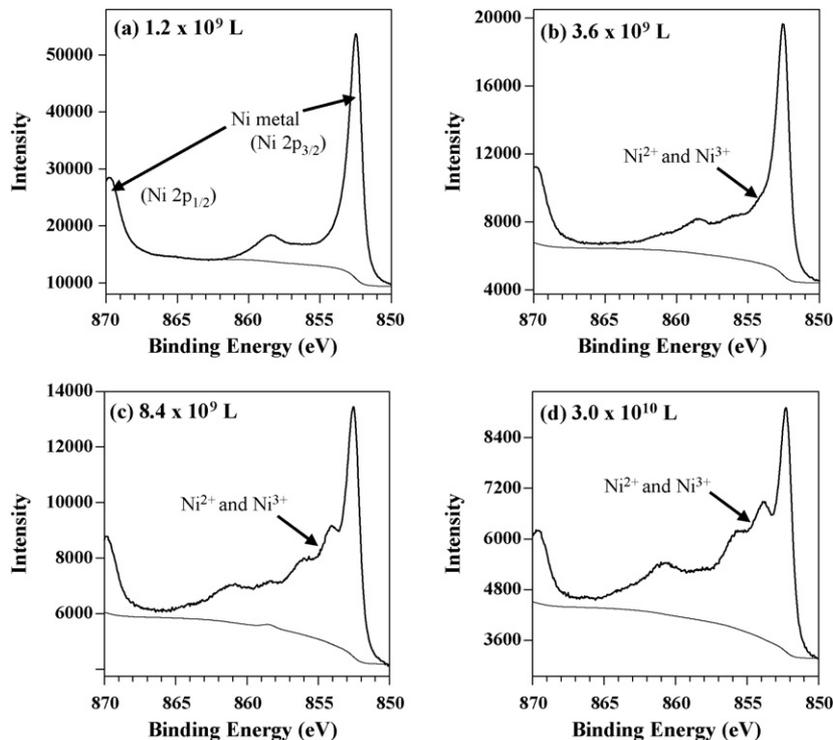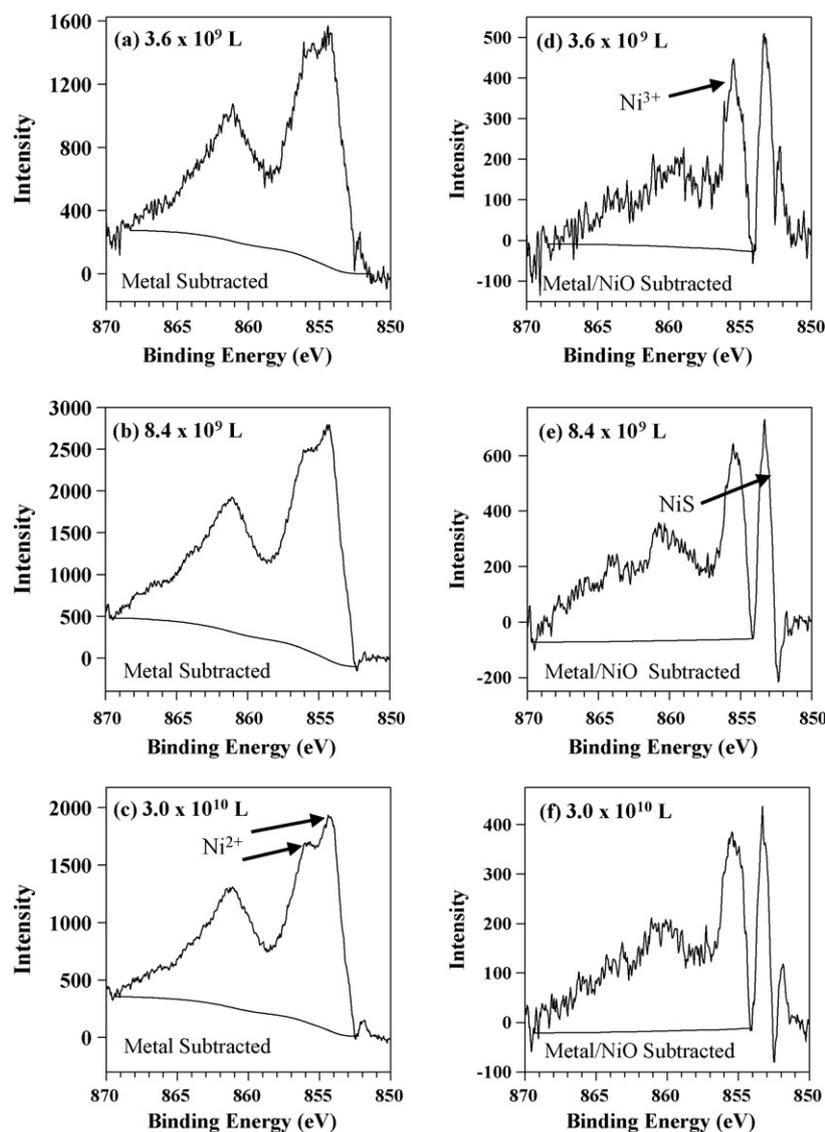

Fig. 4. High-resolution Ni 2p$_{3/2}$ spectra collected after (a) 1.2×10^9 L, (b) 3.6×10^9 L (c) 8.4×10^9 L and (d) 3.0×10^{10} L of exposure to H$_2$O at 300 °C. A small contribution from the metal Ni 2p$_{1/2}$ peak is visible on all spectra.

Fig. 5. Ni $2p_{3/2}$ spectra with the Ni metal component subtracted following exposures of (a) 3.6×10^9 L, (b) 8.4×10^9 L and (c) 3.0×10^{10} L of H_2O vapour. A doublet structure of the main line is visible, suggesting the formation of NiO. The resulting spectra following removal of the NiO contributions for doses of (d) 3.6×10^9 L, (e) 8.4×10^9 L and (f) 3.0×10^{10} L of H_2O vapour are also shown. A small signal from NiS is also visible at the low BE end of the spectrum. The remaining Ni signal resembles that of NiOOH, a Ni^{3+} containing material.

doublet shape of the NiO main line suggest the presence of an additional component near 856 eV. To further investigate the Ni species present following H_2O vapour exposures the NiO component was removed and the resulting spectra are shown in Fig. 5(d–f). In all the subtracted spectra two additional components near 856 eV and 853 eV were found. The peak near 856 eV is thought to be the result of a Ni^{3+} species at the very near surface brought on by the presence of Ni vacancies. A similar result had been observed following the exposure of Ni metal surfaces to O_2 gas at 25 °C and during the initial stages of reaction at 300 °C [14]. The sharp peak near 853 eV is thought to be the result of sulfur (S) contamination. All of the oxidised surfaces were found to contain between 1 and 5% S. Although no high-resolution analysis of the S 2p region was undertaken the BE associated with these S species from XPS survey spectra was found to range between 162.1 eV and 162.9 eV, indicative of a nickel sulfide (NiS) [30].

From the subtraction results shown above it is evident that any analysis of the Ni 2p envelopes is complicated by the presence of Ni metal, Ni^{2+} (from NiO), Ni^{3+} (from defective NiO) and NiS on each surface. Fitting of the Ni 2p spectra entailed using contribu-

tions from Ni metal, NiO and NiOOH components [20]. The NiOOH component was chosen to represent the defective NiO because it contains both Ni^{3+} species and has a similar line shape to the subtracted spectra shown in Fig. 5(d–f). The surface percentages calculated for the Ni metal, Ni^{2+} and Ni^{3+} species obtained from these peak fittings are presented in Table 1. It appears that following doses of 3.6×10^9, 8.4×10^9 and 3.0×10^{10} L each surface contains between 3 and 5% Ni^{3+} (Figs. 4(b–d)). For the case of the lowest dose, a Ni^{3+} component of around 1% with a large uncertainty was determined.

Analysis of the O 1s envelopes collected from surfaces subjected to H_2O exposures of 3.6×10^9 L or greater showed two major peaks at 529.4 ± 0.1 eV and 531.2 ± 0.1 eV (Fig. 6(b–d)). The first peak is assigned to O^{2-} and the second peak is believed to be the result of an O (def) species. When the combined intensities of both the O^{2-} and O (def) species are compared to the surface Ni^{2+} and Ni^{3+} percentages obtained from the Ni 2p analysis, O/Ni ratios of close to 1 are observed (see Table 1). This result suggests that the films formed here are similar in structure to that of the reference NiO. The peak attributed to O (def) cannot represent a bound OH^- species

Table 1
Near-surface compositions of Ni and O species for surfaces exposed to H_2O vapour at 300 °C.

| Dose (L)	Ni metal (%)	Ni^{2+} (%)	Ni^{3+} (%)	$Ni^{2+} + Ni^{3+}$ (%)	O^{2-} (%)	O (def) (%)	$O^{2-} + O$ (def) (%)	O/Ni
1.2×10^{9} [a]	71	–	1	1	–	1	1	1
3.6×10^{9}	46	12	4	16	8	10	18	1.1
3.6×10^{9}	41	14	5	19	9	11	20	1.1
8.4×10^{9}	26	20	3	23	16	8	24	1.0
8.4×10^{9}	26	18	5	23	13	14	27	1.2
3.0×10^{10}	26	20	5	25	15	14	29	1.2
3.0×10^{10}	20	21	4	25	16	12	28	1.1

[a] Large uncertainty in the measurement due to the small amount of oxide present.

since reference OH⁻ compounds studied had O/Ni ratios between 1.6 and 2.6 (see Appendix A). For the O 1s spectrum collected following a dose of 1.2×10^{9} L the peak at 531.3 eV was assigned to O (def). The O/Ni ratio calculated for this surface was found to be 1 (Table 1). In this case the presence of an adsorbed O species cannot be completely ruled out due to both the large uncertainty in the Ni 2p fit above and the QUASES™ analysis described below. There is no evidence for the presence of H_2O (ads) on any of these surfaces at this temperature. This suggests that any H_2O reactant dissociates quickly on the surface and is not observed as an intermediate.

The oxide thicknesses on all samples exposed to H_2O vapour at 300 °C were calculated using QUASES™ 'Analyze'; the results are tabulated in Table 2. No 'Analyze' data was reported for the surface exposed to a dose of 1.2×10^{9} L, as the background could not be modeled. This indicates that either, very little oxide was formed, or that an adsorbed O species is present here. The overlayer thickness for this sample was calculated using the Strohmeier formula. From Table 2, exposures of 3.6×10^{9} L of H_2O vapour at 300 °C lead to a determined average oxide thickness of 0.6 nm. In a previous publication by our group, the same dose of O_2 molecules at 300 °C produced films averaging 4.5 nm thick [14]. It is evident that the oxides grown following exposures to H_2O vapour are much thinner compared to similar doses of O_2. Further examination of the 'Analyze' results shows that there was very little change in the oxide thicknesses at doses of greater than 8.4×10^{9} L. It appears that the oxidation rate has reduced significantly between these two exposures, and the surface is becoming passivated.

All Ni surfaces oxidised at 300 °C were also subject to analysis using QUASES™ 'Generate' and modeled overlayers of NiO. Fig. 7 shows a representative fit for a Ni surface exposed to H_2O for a dose of 3.0×10^{10} L. The best fit was obtained using the 'island active substrate' depth profile for the Ni metal reference spectrum and the 'buried layer' depth profile for the NiO reference spectrum. Here there is a very good overlap between the reference and experimental spectra within the modeling KE range 940–1060 eV. The peak centred near 1033 eV is assigned to Ni 2s photoelectrons in the Ni metal and NiO reference spectra, as well as in the experimental spectrum. A peak found near 965 eV on both the NiO reference and experimental spectra is the result of a sodium (Na) impurity. All of the oxidised surfaces were modeled using these same parameters, and representative depth profiles of the cross-sections of the surface regions following exposures of 3.6×10^{9}, 8.4×10^{9} and 3.0×10^{10} L are shown in Fig. 8. The 'Generate' analysis suggests
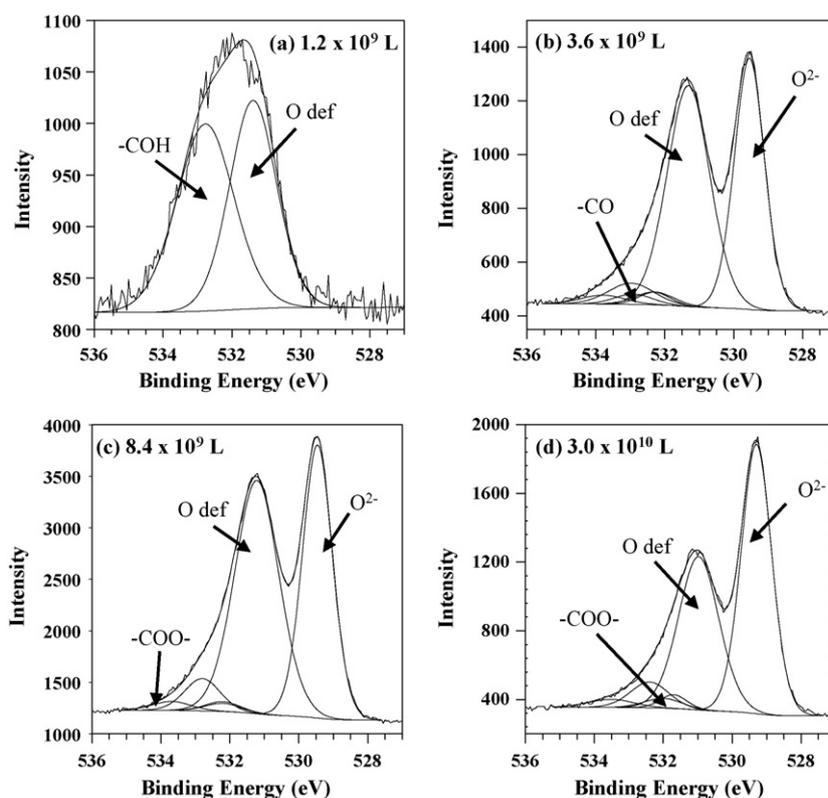
Fig. 6. High-resolution O 1s spectra for exposures of (a) 1.2×10^{9} L, (b) 3.6×10^{9} L (c) 8.4×10^{9} L and (d) 3.0×10^{10} L. Two O species bound to Ni are proposed: O^{2-}, O (def), along with –COH, –CO and –COO– adsorbates. The spectrum in (a) is noisy due to the small amount of O present.

Table 2
Calculated film thickness and surface coverage using QUASES™ and Strohmeier formula.

Dose of H_2O vapour (L)	'Analyze' oxide thickness (nm)	'Generate' oxide thickness (nm)	'Generate' oxide surface coverage (%)	Strohmeier oxide thickness (nm)
1.2×10^{9} [a]	–	–	–	0.2
3.6×10^{9}	0.6	0.6	20	0.5
3.6×10^{9}	0.7	0.6	40	0.6
8.4×10^{9}	1.2	1.2	75	1.1
8.4×10^{9}	1.3	1.3	65	1.2
3.0×10^{10}	1.4	1.4	75	1.2
3.0×10^{10}	1.3	1.3	80	1.4

[a] Surface overlayer calculated with the Strohmeier formula.
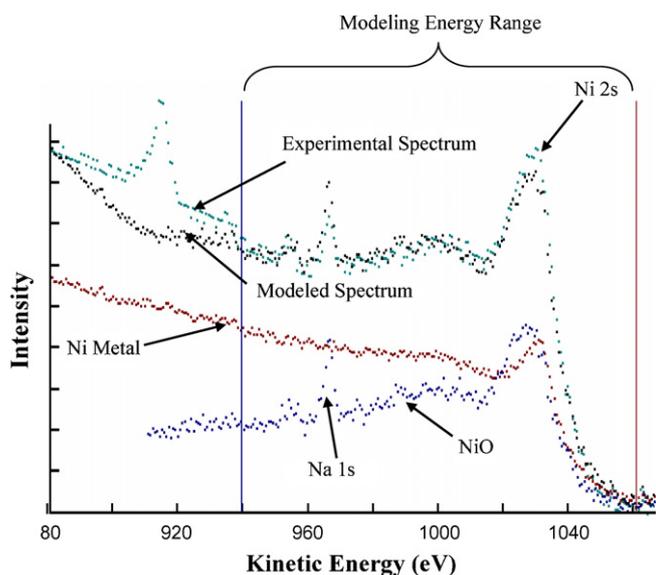
Fig. 7. QUASES™ 'Generate' fit for a Ni metal surface exposed to H_2O vapour for a dose of 3.0×10^{10} L. The experimental spectrum was fit using reference spectra acquired from a clean Ni metal surface and polycrystalline NiO powder. The surface was modeled using the 'island active' profile for the Ni metal component and the 'buried layer' profile for the NiO powder. The peaks located near 1033 eV and 965 eV are assigned to Ni 2s and Na 1s photoelectrons, respectively.

that oxidation proceeds through island growth across the surface with the formation of localised NiO clusters. The advantage to using the 'Generate' program is that it allows for a more detailed modeling of the near surface. While both 'Analyze' and 'Generate'
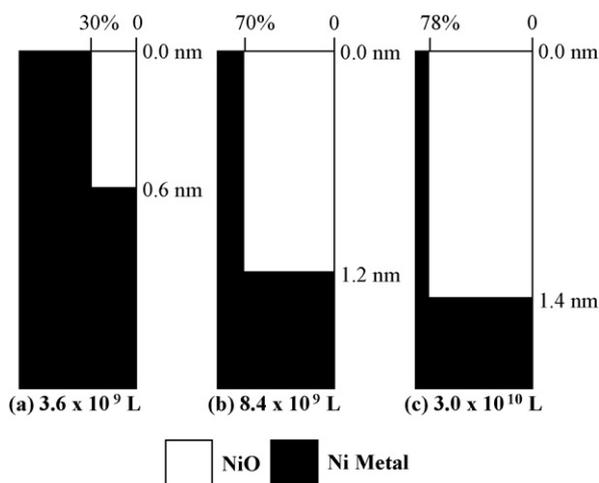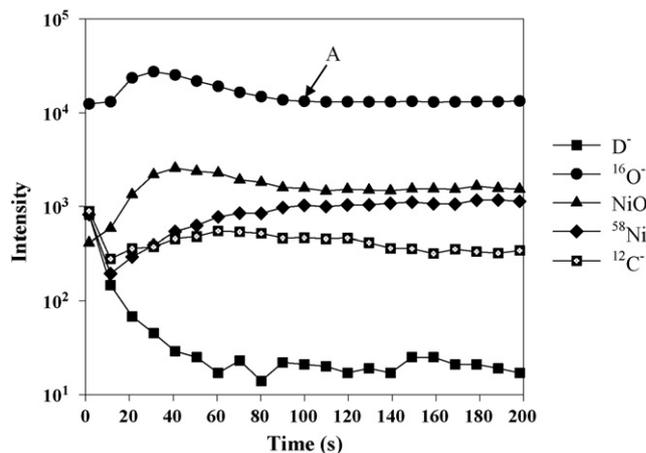
can be used to accurately model non-uniform overlayers the later program also yields compositional information. 'Generate' uses reference spectra collected from samples with known composition to map the in-depth concentration profile of atoms in a surface [10–12]. The results show that with increasing vapour exposure the oxide islands cover more of the analysed area. Following doses of 8.4×10^9 and 3.0×10^{10} L average surface coverages of 70 and 78% were determined. Comparison of both the QUASES™ 'Analyze' and 'Generate' results to the Strohmeier calculated values show very close agreement of film thickness. All QUASES™ 'Generate' data is shown in Table 2.

The shallow SIMS depth profile collected from a surface exposed to D_2O for approximately 1.2×10^9 L is shown in Fig. 9. The point labeled (A) represents the oxide/bulk metal interface that was reached after about 100 s of sputtering as the signals from each secondary ion fragments has become constant. The D fragment is clearly associated with a species at or near the outer surface, and the signal diminishes sharply with depth into the surface. In the case of the Ni–D_2O reaction, it appears that the D is confined to the outer atomic layers.

The oxide thicknesses measured by QUASES™ were plotted against dose using the three kinetic models [31–34] parabolic ($R^2 = 0.99$), direct logarithmic ($R^2 = 0.98$) and inverse logarithmic ($R^2 = 0.80$). The logarithmic model seems more sensible in view of the evidence for Ni^{3+} hole formation. The thickness measured for the highest H_2O dose does not fit the same mechanistic regime; from this dose it appears that the surface has become effectively unreactive toward H_2O. It is interesting to compare the oxide growth curves for Ni exposed to O_2 at 300 °C [14] and H_2O at 300 °C (Fig. 10). For the O_2 exposures the reaction was found to follow a parabolic relationship with dose and the rate of growth for the O_2 reaction is four times that for the initial stages for the H_2O vapour reaction.

Fig. 8. Depth profiles through the near surface areas of Ni metal samples exposed to H_2O vapour for (a) 3.6×10^9 L, (b) 8.4×10^9 L, and (c) 3.0×10^{10} L. There is one distinct oxide phase identified: NiO and the 'Generate' analysis in all cases indicated island oxide growth.

Fig. 9. ToF-SIMS depth profile of a polycrystalline Ni metal surface exposed to approximately 1.2×10^9 L of D_2O vapour in the temperature range of 300–400 °C. The negative secondary ions monitored were D^-, $^{16}O^-$, NiO^-, $^{58}Ni^-$ and $^{12}C^-$.
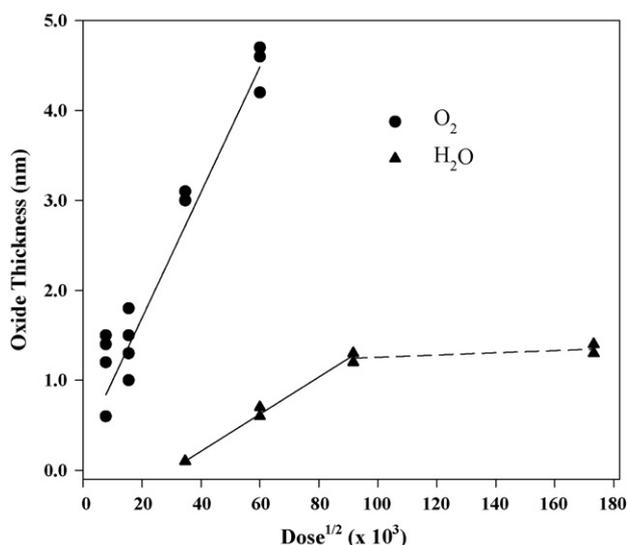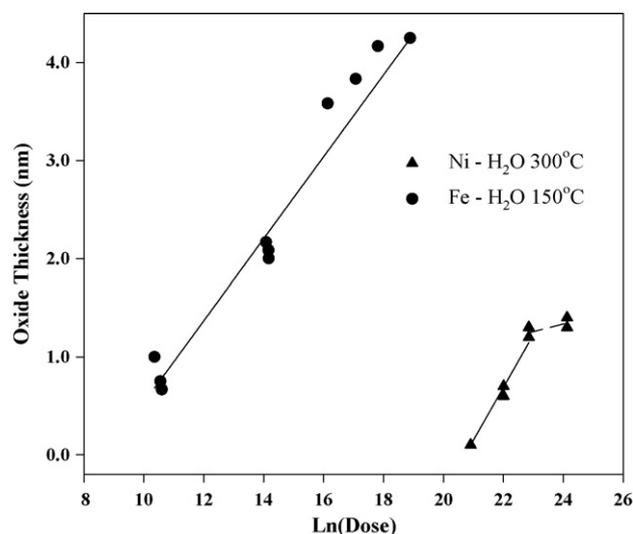
Fig. 10. Comparison of oxide growth curves for Ni metal reacted with O_2 [38] and H_2O. The oxide thicknesses in each case are plotted *vs.* dose$^{1/2}$.

Fig. 12. Comparison of the rates of oxidation of polycrystalline Ni metal surfaces exposed to H_2O vapour at 300 °C with the oxidation of polycrystalline Fe surfaces dosed with H_2O at 150 °C [39]. The rate of Ni oxidation is found to be much slower when compared to that of Fe.

Second, there is no evidence for termination of reactivity for the O_2 reaction (at least within this dose range), while this is clearly evident for the H_2O reaction after the formation of a thin oxide film. Finally, the H_2O reaction only begins to cause detectable oxide growth after a very large dose.

The H_2O vapour Ni reaction was also studied briefly at 25 °C. The Ni $2p_{3/2}$ and O 1s spectra collected following a dose of 3.0×10^9 L are shown in Fig. 11. As with the 300 °C exposures a small portion of the metal Ni $2p_{1/2}$ line is also present within the BE window shown here. Fitting of the Ni 2p envelope indicates that very little oxidised Ni is present. The corresponding O 1s spectrum has a peak at 531.1 eV, but in this case there is no equivalent amount of oxidised Ni. We therefore assign this to an oxidic species adsorbed on the metal, prior to its place exchange and incorporation as an oxide. The existence of an O (ads) is unlikely: our previous study of Ni oxidation with O_2 showed that this species is highly reactive, with oxide nucleation occurring after relatively small doses [14]. Thus, the oxidic species is likely to be an OH (ads). Its presence suggests that its rate of conversion to an oxide is much slower at this temperature compared to 300 °C as no detectable oxide has formed following this dose.

A comparison of the H_2O water reaction processes on clean Fe [7] and Ni surface under high flux is shown in Fig. 12. Although the temperature used for the Fe reaction (150 °C) differed from that used for Ni, the effects of temperature on the oxide thickness *versus*

dose are not important on the scale shown. The most important conclusion is that the time taken to begin nucleation and growth of oxide on Ni is much longer than for Fe. In the cases of both Fe and Ni oxidised under high flux conditions, the recombination and desorption reactions compete successfully with place exchange for most reactant species on the surface.

The lack of spectral evidence for the presence of any H_2O (ads) species on these surfaces suggests quick dissociation of this reactant upon interaction with Ni metal at both 25 °C and 300 °C. On the basis of these observations we propose that the H_2O quickly dissociates into OH (ads) and H (ads) species. However, the initial formation of a thin oxide film was found to occur much slower as compared to the similar exposures of O_2 to Ni, where the reactive intermediate was shown to be O (ads) [14] (see Fig. 10). The rate-determining step for this Ni–H_2O reaction is thought to be the slow place exchange of an OH (ads) with Ni metal and subsequent loss of H. Some of this H may become trapped in the oxide vacancies (Ni holes) and retard the migration of such vacancies, thus slowing the oxide growth even further. Analysis of the depth profile collected with the ToF-SIMS did show the presence of some H at the surface. A similar explanation was also used to explain the reduction in oxidation rate of Fe surfaces following exposure to H_2O vapour [7–9].
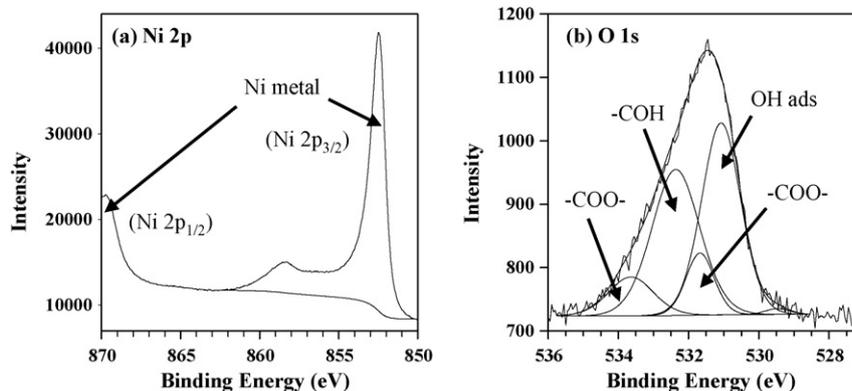
Fig. 11. High-resolution (a) Ni $2p_{3/2}$ and (b) O 1s spectra collected following a H_2O vapour exposure of 3.0×10^9 L at 25 °C. There is no evidence to suggest any Ni^{2+} or Ni^{3+} has formed. The O 1s scan does show the presence of four O species: OH (ads), –COH, –CO and –COO–. The start of the Ni $2p_{1/2}$ line is visible at high BE.

Examples showing the stability of OH (ads) species on transition metal surfaces are available in the literature [6,35–37]. Andersson et al. have studied the dissociation of H_2O (ads) on single crystal (1 1 0) copper (Cu) surfaces following low doses of H_2O vapour ($<3.0 \times 10^7$ L) [35,36]. They showed using XPS that that within the temperature range of 150 °C and 250 °C the only O species present was that of an OH (ads), while between 0 °C and 150 °C both H_2O (ads) and OH (ads) were present. A similar result was also reported by Schiros et al. on single crystal (1 1 1) platinum (Pt) surfaces exposed to low doses of H_2O vapour at temperatures below 0 °C [37].

In the case of the Ni–H_2O reactions carried out at 300 °C described above there was no spectral evidence to support the presence of any OH (ads) species on the metal surfaces (Fig. 6). These surfaces were subjected to much larger doses ($\geq 1.2 \times 10^9$ L) than the Cu and Pt single crystals [35–37]. It is therefore possible that any OH (ads) species that may have been present has reacted to form an oxide. The O 1s spectrum (Fig. 11b) collected from a Ni surface exposed to H_2O vapour at 25 °C did show the presence of OH (ads) at this temperature. However, unlike with the cases of Cu and Pt a peak resulting from H_2O (ads) was not detected. Heras and Albano have shown that H_2O (ads) readily undergoes desorption from Ni metal and Ni oxidised surfaces even at low temperatures [4,5].

The termination of this reaction was found to occur following the formation of very thin films. We propose that the decomposition of OH (ads) cannot be sustained in the absence of a metallic surface. Therefore, after the metal phase becomes effectively unavailable to an OH (ads) reactant, the reaction is terminated and the surface is passivated. This could correspond to the 1–1.4 nm thick film of NiO observed here. This conclusion is supported by the work of Heras and Albano in which they showed that H_2O (ads) would decompose on Ni metal, but not on oxidised or passivated surfaces [4,5]. This result could have implications for Ni surfaces in high temperature steam conditions. Under reducing conditions, where no O is present, the surface layer would be expected to be composed of a very thin film of oxide that does not grow with extended exposure. The rate of reaction of Fe and H_2O is much faster when compared to that of Ni metal. In the case of the Fe reaction, iron hydroxide ($Fe(OH)_2$) and iron oxy-hydroxide (FeOOH) species were found to be stabilised on the surface [7,8]. Although it is believed that small amounts of OH (ads) were found on Ni, the analogous $Ni(OH)_2$ and NiOOH species were not present. Such species may act to increase the rate of reaction with H_2O on Fe, by increasing the number of possible reaction pathways.

4. Conclusion

The initiation and subsequent rate of oxidation of polycrystalline Ni by H_2O vapour is slower than with O_2 gas and is limited to a few surface atomic layers under the conditions studied. What oxidation occurs is the result of a reaction of OH (ads) with metallic Ni to form NiO and H, some of which is incorporated in the film. The reaction terminates after all metallic sites are covered. The rate at which H_2O is converted to oxide is many orders of magnitude slower on Ni than it is on Fe under similar conditions.

Acknowledgements

Table A1
Ni and O surface concentrations for Ni metal surfaces exposed to doses of H_2O vapour and O_2 gas.

Reactant gas and temperature °C	Dose of H_2O vapour (L)	Oxidised Ni on surface (%)	O^{2-} and O (def) present (%)	O/Ni Ratio	Oxide thickness (nm)
H_2O/300	1.2×10^9	1	1	1	0.2
	3.6×10^9	16	18	1.1	0.6
	3.6×10^9	19	20	1.1	0.7
	8.4×10^9	23	24	1.0	1.2
	8.4×10^9	23	27	1.2	1.3
	3.0×10^{10}	25	29	1.2	1.4
	3.0×10^{10}	25	28	1.1	1.3
O_2/25	6.0×10^8	2	2	1	0.2
	6.0×10^8	0.9	3	3	0.1
	6.0×10^8	4	5	1.2	0.2
	1.5×10^9	4	8	2	0.4
	1.5×10^9	13	22	1.7	0.8
	3.0×10^9	10	17	1.7	0.7
	3.0×10^9	17	22	1.3	0.9
	3.0×10^9	21	25	1.2	1.1
	6.0×10^9	18	24	1.3	1.3
	6.0×10^9	10	19	1.9	0.9
O_2/300	6.0×10^7	21	12	1.1	1.2
	6.0×10^7	7	10	1.4	0.6
	6.0×10^7	24	28	1.2	1.4
	6.0×10^7	25	28	1.1	1.5
	2.4×10^8	25	27	1.1	1.5
	2.4×10^8	19	20	1.1	1.0
	2.4×10^8	22	28	1.3	1.3
	2.4×10^8	33	29	0.89	1.8
	1.2×10^9	37	37	1.0	3.1
	3.6×10^9	49	40	0.81	4.7
	3.6×10^9	43	41	0.95	4.2
	3.6×10^9	44	39	0.89	4.6

The spectra for the O_2 exposed surfaces was collected and published previously [14]. In the previous publication the O (def) peak had been interpreted solely as O (ads).

Table A2
Ni 2p and O 1s surface percentages for Ni-containing powders.

Sample	O^{2-} (%)	O (def) (%)	OH– (%)	Total O (%)	Ni (%)	O/Ni
NiO-1[a]	28	12	–	40	38	1.1
NiO-2[a]	28	11	–	39	34	1.1
NiO-3[a]	29	11	–	40	37	1.1
NiO-4	29	11	–	40	35	1.1
NiO-5	29	10	–	39	36	1.1
NiO-6	28	10	–	38	35	1.1
$Ni(OH)_2$-1	–	–	53	53	20	2.6
$Ni(OH)_2$-2	–	–	51	51	31	1.6
$Ni(OH)_2$-3	–	–	51	51	29	1.8
$Ni(OH)_2$-4	–	–	51	51	31	1.6
$Ni(OH)_2$-5	–	–	57	57	37	1.5
γ-NiOOH	17	–	22	39	21	1.9
β-NiOOH	8	–	30	38	20	1.9

[a] The powders used for these experiments were received packed under Ar and preparation for XPS analysis was carried out in a glove box filled with Ar attached to the XPS instrument. All other samples were stored in air prior to introduction to the XPS. Samples were prepared by pressing some NiO powder into indium foil using a glass slide.

Appendix A. Comments on the XPS identification of nickel oxide species

While both Ni 2p and O 1s line shapes can give useful chemical information on the oxides formed, it has been very difficult to derive information that is non-ambiguous. For example, in the course of interpreting the spectra in this study we have at various times identified the O 1s peak at 531.2 eV as due to OH– (in $Ni(OH)_2$), O (ads) and "defective oxygen" (an oxygen adjacent to a defect site or Ni vacancy). The ambiguity stems from the overlapping BE shifts of these species.

We now favour the last interpretation from the following argument. We find a relationship between the corrected intensities for non-metallic Ni (essentially Ni^{2+} and Ni^{3+}) in Ni 2p spectra and the combined intensities of the O 1s peaks at 529.4 eV and 531.2 eV. The ratio of these intensities is shown in Table A1 for NiO spectra produced in this work with H_2O and spectra from our previous paper on the oxidation of Ni with O_2 [14]. Refitting of the Ni 2p and O 1s spectra collected, as part of the Ni–O_2 investigation was undertaken using the same parameters used to monitor the Ni–H_2O reaction. For most cases the reaction products between H_2O and Ni and the reaction products of Ni and O_2 at 300 °C, there is an O/Ni ratio close to 1. The ratio of O/Ni appears to drop following the longest exposures to O_2, suggesting that these films are O deficient, most likely at the oxide/metal interface. The majority of the surfaces exposed to O_2 at 25 °C show O/Ni ratios of much greater than 1. The O_2 gas used during this oxidation study was of high-purity (99.99%) so the possibility the presence of substantial amounts of adsorbed or bound OH is unlikely. Thus the intensity of the peak 531.2 eV may then result from a combination of both O (def) and O (ads) species. It should be noted that in Ref. [14] the peak at 531.2 eV on all Ni surfaces was incorrectly labeled as purely and O (ads) species.

Samples of powdered NiO (air and non-air exposed), $Ni(OH)_2$, γ-NiOOH and β-NiOOH were also analysed and the calculated O/Ni ratios obtained are shown in Table A2. Earlier work by Norton et al. [1], Roberts and Smart [22], Roberts [24] and Carley et al. [23,25] all assign this high BE peak to the presence of a defective NiO-essentially reaching the same conclusion as we do here.

References

[1] P.R. Norton, R.L. Tapping, J.W. Goodale, Surf. Sci. 65 (1977) 13.
[2] C. Benndorf, C. Nöble, M. Rüsenberg, F. Thieme, Appl. Surf. Sci. 11/12 (1982) 803.
[3] C. Benndorf, C. Nöble, F. Thieme, Surf. Sci. 121 (1982) 249.
[4] J.M. Heras, E.V. Albano, Appl. Surf. Sci. 17 (1983) 207.
[5] J.M. Heras, E.V. Albano, Appl. Surf. Sci. 17 (1983) 220.
[6] A.F. Carley, S. Rassias, M.W. Roberts, Surf. Sci. 135 (1983) 35.
[7] A.P. Grosvenor, B.A. Kobe, N.S. McIntyre, Surf. Sci. 572 (2004) 217.
[8] A.P. Grosvenor, J.T. Francis, B.A. Kobe, N.X. McIntyre, Surf. Interface Anal. 37 (2005) 495.
[9] B.L. Maschhoff, N.R. Armstrong, Langmuir 7 (1991) 693.
[10] S. Tougaard, Surf. Interface Anal. 26 (1998) 249.
[11] S. Tougaard, QUASES™, Version 4.4, Software for Quantitative XPS/AES of Surface Nano-Structures by Analysis of the Peak Shape Background, 2000.
[12] S. Tougaard, User's Guide, QUASES™, Version 4.4, Software for Quantitative XPS/AES of Surface Nano-structures by Analysis of the Peak Shape Background, 2000.
[13] A.P. Grosvenor, B.A. Kobe, N.S. McIntyre, Surf. Sci. 565 (2004) 151.
[14] B.P. Payne, A.P. Grosvenor, M.C. Biesinger, B.A. Kobe, N.S. McIntyre, Surf. Interface Anal. 39 (2007) 582.
[15] A.P. Grosvenor, B.A. Kobe, N.S. McIntyre, S. Tougaard, W.N. Lennard, Surf. Interface Anal. 36 (2004) 632.
[16] A.P. Grosvenor, B.A. Kobe, N.S. McIntyre, Surf. Interface Anal. 36 (2004) 1637.
[17] T. Do, N.S. McIntyre, Proceedings of the 2nd International Symposium on Aluminum Surface and Technology (ASST 2000), Manchester, England, UK, May 21–25, 2000, p. 37.
[18] N. Fairley, CasaXPS Version 2.2.107, 1999–2005.
[19] G. Beamson, D. Briggs, High-resolution XPS of Organic Polymers The Scienta ESCA300 Database, John Wiley and Sons, Toronto, 1992 (Appendices 1–3).
[20] M.C. Biesinger, B.P. Payne, L.W.M. Lau, A. Gerson, R.St.C. Smart, Surf. Interface Anal. 41 (2009) 324.
[21] A.P. Grosvenor, M.C. Biesinger, R.St.C. Smart, N.S. McIntyre, Surf. Sci. 600 (2006) 1771.
[22] M.W. Roberts, R.St.C. Smart, J Chem. Soc., Faraday Trans. 80 (1984) 2957.
[23] A.F. Carley, P.R. Chalker, M.W. Roberts, Proc. R. Soc. Lond. A 399 (1985) 167.
[24] M.W. Roberts, Surf. Sci. 299/300 (1994) 769.
[25] A.F. Carley, S.R. Grubb, M.W. Roberts, J. Chem. Soc., Chem. Commun. (1984) 459.
[26] NIST Electron Inelastic Mean Free Path Database (Version 1.1)©, U.S. Secretary of Commerce., 2000.
[27] S. Tanuma, C.J. Powell, D.R. Penn, Surf. Interface Anal. 11 (1998) 577.
[28] B.R. Strohmeier, Surf. Interface Anal. 15 (1990) 51.
[29] Ion-ToF(GmbH), IONSPEC, v. 3.14.9, Ion-ToF, Münster, Germany, 1995–2000.
[30] H.W. Nesbitt, D. Legrand, G.M. Bancroft, Phys. Chem. Miner. 27 (2000) 357.
[31] F.P. Fehlner, N.F. Mott, Oxidation of Metals and Alloys; Papers Presented at a Seminar of the American Society for Metals, October 17 and 18, 1970, American Society for Metals, Metals Park, OH, 1971, p. 37.
[32] F.P. Fehlner, M.J. Graham, in: P. Marcus, J. Oudar (Eds.), Corrosion Mechanisms in Theory and Practice, Marcel Decker Inc., New York, 1995 (Chapter 4).
[33] N. Cabrera, N.F. Mott, Rep. Prog. Phys. 12 (1948–1949) 163.
[34] F.P. Fehlner, N.F. Mott, Oxidat. Met. 2 (1970) 59.
[35] K. Andersson, G. Ketteler, H. Bluhm, S. Yamamoto, H. Ogasawara, L.G.M. Pettersson, M. Salmeron, A. Nilsson, J. Phys. Chem. C 111 (2007) 14493.
[36] K. Andersson, G. Ketteler, H. Bluhm, S. Yamamoto, H. Ogasawara, L.G.M. Pettersson, M. Salmeron, A. Nilsson, J. Am. Chem. Soc. 130 (2008) 2793.
[37] T. Schiros, L.-Å. Näsland, K. Andersson, J. Gyllenpalm, G.S. Karlberg, H. Ogasawara, L.G.M. Pettersson, A. Nilsson, J. Phys. Chem. C 111 (2007) 15003.
[38] B.P. Payne, A.P. Grosvenor, M.C. Biesinger, B.A. Kobe, N.S. McIntyre, Structure and Growth of Oxides on Polycrystalline Nickel Surfaces, p. 588. Reprinted from Surface and Interface Analysis, vol. 39, Copyright 2007, with permission from Wiley InterScience.
[39] A.P. Grosvenor, B.A. Kobe, N.S. McIntyre, Studies of the Oxidation of Iron by Water Vapour Using X-ray Photoelectron Spectroscopy and QUASES™, p. 225. Reprinted from Surface Science, vol. 572, Copyright 2004, with permission from Elsevier.